Asian Journal of Chemistry; Vol. 28, No. 1 (2016), 221-229

ASIAN JOURNAL OF CHEMISTRY

http://dx.doi.org/10.14233/ajchem.2016.19355

Influence of Zinc Additive and pH on Electrochemical Behaviour of β-Nickel Hydroxide in Nickel Based Secondary Batteries

C.R. RAVI KUMAR[1,*], P. KOTTEESWARAN[2], M.S. SANTOSH[3], B. SHRUTHI[4], V. BHEEMARAJU[4], M.S. SHIVAKUMARA[5] and H.P. NAGASWARUPA[1]

[1]Research Centre, Department of Chemistry, East West Institute of Technology, Bangalore-560 091, India
[2]Department of Chemistry, Renganayagi Varatharaj College of Engineering, Salvarpatti-626128, India
[3]Centre for Emerging Technologies, Jain University, Jain Global Campus, 45th km, NH-209, Jakkasandra Post, Kanakapura Taluk, Ramanagaram-562 112, India
[4]Department of Chemistry, Dr. Ambedkar Institute of Technology, Bangalore-560 056, India
[5]Department of Chemistry, ACS College of Engineering, Bangalore-560 074, India

*Corresponding author: E-mail: ravicr101@yahoo.com

Received: 21 May 2015; *Accepted*: 1 July 2015; *Published online*: 5 October 2015; AJC-17579

Nickel(II) hydroxide has been prepared by co-precipitation method with various concentrations of Zn additives (2, 4, 6 and 8 wt %) under different pHs (8, 9, 10 and 11). The elemental composition of zinc substituted nickel hydroxide samples were studied using energy dispersive X-ray analysis and the β-form of $Ni(OH)_2$ samples were confirmed by X-ray diffraction and Fourier transform infrared spectroscopy. The interlayer distance (c_0) is found to expand with an increase in the percentage of zinc additives. The amount of SO_4^{2-}, CO_3^{2-} and H_2O adsorbed by the crystals and the thermal stability of β-$Ni(OH)_2$ are dependent on the pH. Under relatively high pH value, the synthesized nickel hydroxide materials possess an increasing degree of order and crystallinity, lower thermal stability, lower taping density and higher Ni composition. The electrochemical properties of the synthesized $Ni(OH)_2$ materials were analyzed using cyclic voltammetry and electrochemical impedance spectroscopy. It is evident from the experimental data that the redox reactions exhibit quasi-reversible nature for all electrodes except for electrode C indicating that the charge and discharge process of the latter showed better reversibility compared to other electrodes. The electrochemical studies also indicate that zinc-ion additive is successful in increasing the reversibility of the electrode reaction and also the capacitance of the electrode.

Keywords: Nickel hydroxide, Additive, pH, Interplanar distance, Tapping density, Cyclic voltammetry.

INTRODUCTION

Nickel hydroxide is a critical material in alkaline batteries and has therefore been the subject of many studies in the recent past. It has several desirable and useful characteristics in secondary batteries, namely: (a) it is insoluble ($K_{SP} = 10^{-35}$) in concentrated alkaline electrolyte; (b) during discharge, nickel hydroxide produces a stable and relatively high potential; (c) it can be efficiently charged and discharged multiple times; and (d) with relatively little damage, it can withstand overcharge and over discharge. For these reasons, nickel hydroxide is the most commonly used positive electrode material in alkaline secondary batteries [1-3]. Currently, for various terrestrial applications, Ni/MH batteries are being used successfully. Nickel hydroxide exists in several different forms, each differing in crystal structure and composition. Fig. 1 indicates different phases of $Ni(OH)_2$ as represented by Bode *et al.* [4]; β-$Ni(OH)_2$ is the starting material which on charge transformation leads to β-NiOOH and on further charge or overcharge forms γ-NiOOH; γ-NiOOH transforms to α-$Ni(OH)_2$ on discharge and *vice-versa*.

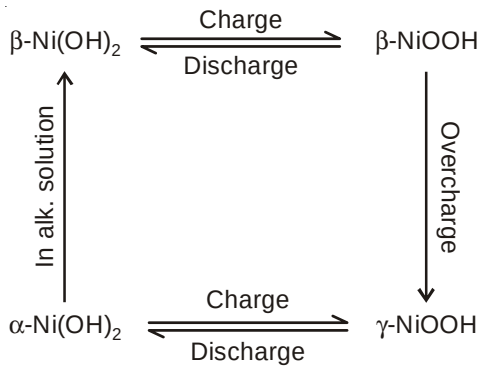

Fig. 1. Different phases of $Ni(OH)_2$

In nickel batteries, two couples of $Ni(OH)_2$ [5,6], α-$Ni(OH)_2$/γ-NiOOH and β-$Ni(OH)_2$/β-NiOOH are used. The first couple discharges more number of electrons than the second one [7,8] but had large storage and discharge capacity. However, α-$Ni(OH)_2$ is not stable in alkaline solution and can be easily converted into β-$Ni(OH)_2$ [9], which is the main drawback of α-$Ni(OH)_2$/γ-NiOOH couple. Due to overcharging or high rate of charging or in concentrated electrolytic solution, β-NiOOH can easily be converted into γ-NiOOH. The formation of γ-NiOOH is associated with volume expansion or swelling of $Ni(OH)_2$ electrode. This results in the enlargement of thickness and surface area of an electrode, finally diminishing the cycle life and capacity of the electrode. In order to accelerate the reactivity and also increase the reversibility of the reaction, additives are incorporated into nickel hydroxide network. For instance, several percentages of Zn, Co or Cd elements were added in the form of solid to $Ni(OH)_2$ to supress the formation of γ-NiOOH [10]. The additives enhance the performance of electrode by suppressing oxygen evolution by increasing the oxygen evolution potential [11]. Compared to Co and Cd that have low rates of reactivity, zinc-ion had better performance [12]. In addition, the fact that Co is considerably expensive and Cd is toxic to the environment makes them unsuitable for use in batteries. It has been reported that the conditions used to add the additives are also responsible for the performance of the electrode. Nickel(II) hydroxide used at higher pH provided much smaller crystallite size, pore volume and low water adsorption ability compared to samples prepared at lower pH leading to high capacity and better electrode characteristics [13]. Through this article, an attempt is made to provide new insights and better understanding of the influence of zinc additive and pH on the electrochemical behaviour of β-$Ni(OH)_2$ samples at varied concentrations. Considering the above facts, the present work is important in the light of providing better alternatives and efficiency in metal based batteries and suggest suitable alternatives for future studies on these lines.

EXPERIMENTAL

Preparation of β-$Ni(OH)_2$ powder without additive: 4 M NaOH solution was added drop wise with continuous stirring into 100 mL of 1 M $NiSO_4$ solution until pH of the solution reached 11. The reaction mixture was maintained at 50 °C and the precipitate under alkaline conditions was kept for ageing for about 15 h. The precipitate was filtered and washed with distilled water until the filtrate became neutral. Later, the precipitate was dried at 90 °C and was ground to a fine powder. This sample was labeled as A.

$$NiSO_4 + 2NaOH \longrightarrow Ni(OH)_2 + Na_2SO_4 \quad (1)$$

Preparation of β-$Ni(OH)_2$ powder with zinc additive: 4 M NaOH solution was added drop wise into 100 mL of 1 M metal salt solution mixture (having appropriate ratio containing 2, 4, 6 and 8 weight % of $ZnSO_4$ with $NiSO_4$ solution) with continuous stirring. The reaction mixture was maintained at 50 °C; the addition of NaOH was stopped at the corresponding pH of different $Ni(OH)_2$ samples. The precipitate in the primary solution was kept for ageing for about 15 h at the same temperature. Later, the precipitate was filtered and washed with distilled water until the filtrate became neutral and was dried at 90 °C. The precipitate was ground to a fine powder and these samples were labeled as given in Table-1.

TABLE-1
DIFFERENT β-$Ni(OH)_2$ SAMPLES

Concentration of additive ($ZnSO_4$, %)	pH levels			
	8	9	10	11
2	B_1	B_2	B_3	B_4
4	C_1	C_2	C_3	C_4
6	D_1	D_2	D_3	D_4
8	E_1	E_2	E_3	E_4

$$(Ni,Zn)SO_4 + 2NaOH \longrightarrow (Ni,Zn)(OH)_2 + Na_2SO_4 \quad (2)$$

Electrochemical studies: Cyclic voltammetry (CV) and electrochemical impedance measurements were carried out using CHI604E electrochemical workstation. For cyclic voltammetric studies, the test electrode was prepared by grinding the combination of 80 % prepared β-nickel hydroxide powder, 15 % graphite powder and 5 % PTFE solution in the form of slurry. The resulting slurry was pasted on nickel mesh. After being coated by the paste, the electrode was dried at 80 °C for 1 h and later, the pasted electrodes were pressed at 20 MPa for 3 min to assure good electrical contact between the nickel mesh and the active material. The backside of the electrode and the wire were insulated using a Teflon tape to obtain an electrode with final dimensions of 2 cm × 1 cm area. A platinum foil was used as a counter electrode; Ag-AgCl electrode was used as a reference electrode and 6 M KOH solution was used as an electrolyte. Prior to CV studies, the electrodes were activated in 6 M KOH solution for 30 min and later, the cyclic voltammograms were obtained. All measurements were carried out at room temperature.

RESULTS AND DISCUSSION

Effect of nickel salts, reaction and drying temperature on the preparation of $Ni(OH)_2$: Higher electrochemical activity was observed for nickel hydroxide synthesized from $NiSO_4$ compared to the those prepared from $Ni(NO_3)_2$ and $NiCl_2$. Adsorption of sulphate ions facilitated the precipitation of $Ni(OH)_2$; this behaviour showed a decrease in the quantity of adsorbed impurities on nickel hydroxide powder [13]. Further to this, at a reaction temperature of 50 °C [14] and a drying temperature of 90 °C [15], the tapping density, discharge capacity and specific capacity of $Ni(OH)_2$ showed better results.

Elemental analysis: The elemental analysis of zinc substituted β-$Ni(OH)_2$ samples were carried out using JEOL 200 kV electron microscope, EDAX spectra of nickel hydroxide samples show the presence of zinc doped nickel. As an active material of electrode, nickel was used as a hydroxide, while zinc was used as an additive to improve the electrochemical properties.

XRD analysis: The characterization of samples were done using Philips X'pert-PRO X-ray diffractometer with graphite monochromatized CuK_α (λ = 1.5418 Å) radiation, at a scan rate of 10° min^{-1} and 2θ steps of 0.05°; the data were collected for the above mentioned nickel hydroxide samples. The XRD patterns of nickel hydroxide samples A, B_1-B_4, C_1-C_4, D_1-D_4 and E_1-E_4 are presented in Fig. 2.

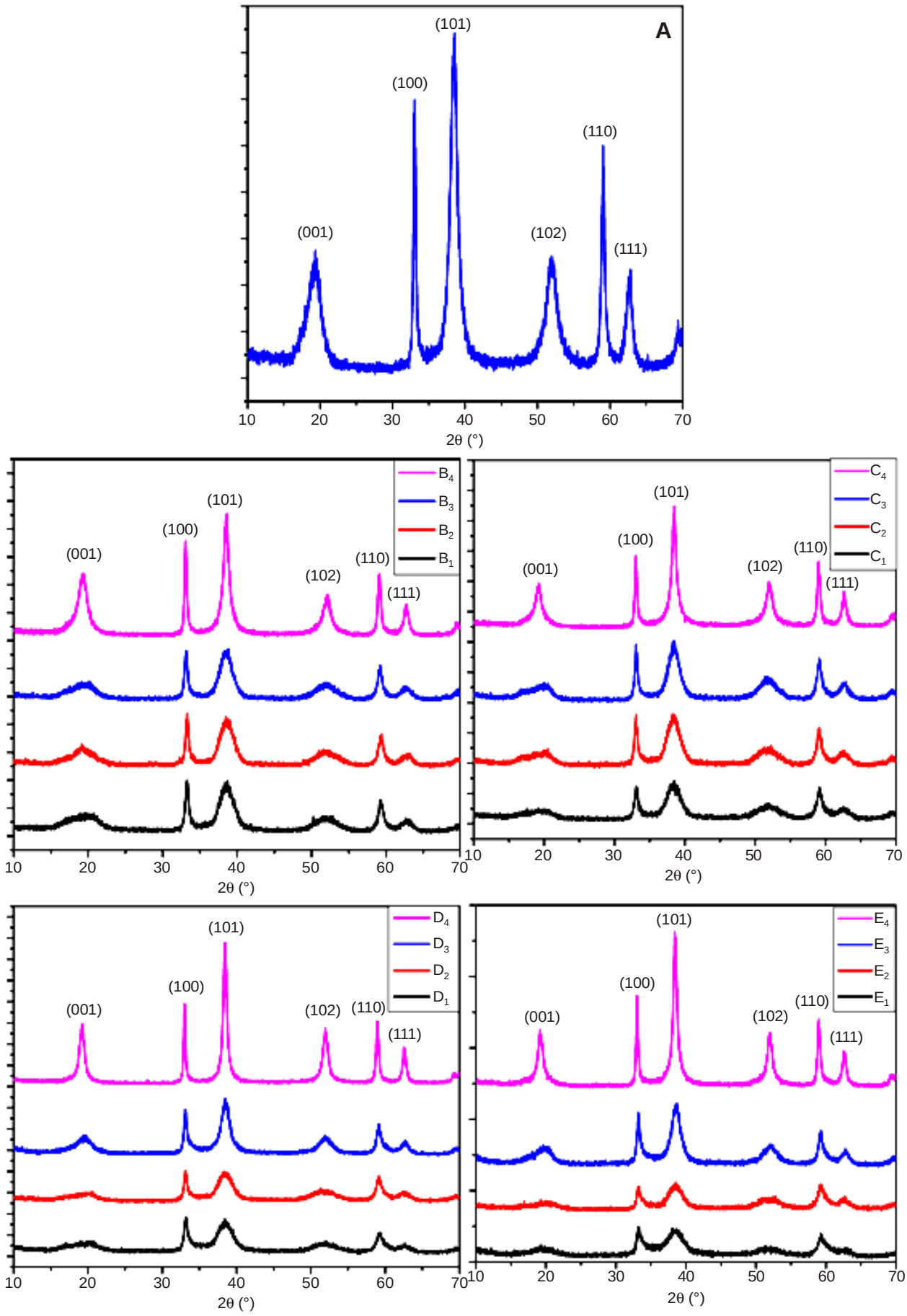

Fig. 3. XRD spectra of nickel hydroxide samples A; (B_1-B_4); (C_1-C_4); (D_1-D_4); (E_1-E_4)

The diffraction peaks at (001)($d_{4.60}$), (100)($d_{2.70}$), (101)($d_{2.34}$), (102)($d_{1.76}$), (110)($d_{1.56}$) and (111)($d_{1.48}$) indicate that all these samples exhibit characteristics of β-$Ni(OH)_2$ phase with a hexagonal unit and a Brucite-type structure [16]. In all samples, the characteristic peaks of zinc were not seen indicating that the zinc component was incorporated into the crystal lattice of β-$Ni(OH)_2$. The full-width of half-maximum intensity (FWHM) of (001), (101) and (102) reflection lines indicate some disorders in the crystal lattice [17,26]. The d_{001} value represents the interlayer distance c_0 of a Brucite-type structure of nickel hydroxide. The d_{100} or d_{110} value corresponds to the Ni-Ni distance α in the layers of nickel hydroxide, where $\alpha = (2/\sqrt{3})\ d_{100}$ or $2d_{110}$ [7,18]. The electrochemical activity was indicated by the (101) line, which was possibly due to the existence of stacking faults in the crystalline lattice of $Ni(OH)_2$ powders [19,20]. The samples A, B_1-B_4, C_1-C_4, D_1-D_4 and E_1-E_4 all have the same β-$Ni(OH)_2$ basic structure. Moreover, their X-ray diffraction patterns represented in Fig. 2 revealed that their detailed microstructural characteristics are considerably different. The peaks corresponding to all the reflections in the X-ray diffraction pattern of samples B_1, B_2 to E_1, E_2 prepared at low pH value are noticeably broadened and/or split as compared to those in the patterns of samples that were prepared at higher pH. This indicates that the samples prepared at low pH are comparatively less ordered and poorly crystallized. On the contrary, sharper reflection peaks were seen for the samples B_3, B_4 to E_3, E_4 which were synthesized at higher pH, indicating an increased degree of ordering and crystallinity. A larger degree of broadening (FWHM) of the peaks corresponding to (001), (101) and (102) reflections were obtained, while the broadening was comparatively smaller for the peaks corresponding to (100) and (110). The exceptional broadening of (001), (101) and (102) reflection lines in the X-ray diffraction patterns of nickel hydroxide materials may be attributed to: (i) crystallite size effects; (ii) increased degree of disordering on account of the existence of crystalline defects, such as proton vacancies, growth faults/stacking faults, or the adsorption of inorganic species (water and anions) [20,21]. The broadening of a few diffraction peaks (*e.g.*, (001) and (h k 0)) is directly related to the crystallite size, D [22].

Scherrer formula $D = 0.9\lambda/B\cos(\theta)$ (where D is the crystallite size, λ represents the X-ray wave length, B is the FWHM and θ is the Bragg angle) was used to estimate the crystallite size perpendicular to various diffraction planes. The FWHM, the *d* values and the peak intensity of samples in (001), (100) and (101) diffraction lines are listed respectively in Table-2. The FWHM of (001) and (101) diffraction lines tend to decrease in the sequence of the samples prepared at higher pH, indicating that the crystallinity of the nickel hydroxide powder tends to increase with increasing pH and also by increasing the percentage of zinc additive. The electrochemical activity is represented by the (101) diffraction line, which increases with increasing pH and the percentage of zinc additive. The d_{001} diffraction line increases with increasing pH and the percentage of zinc additive because Ni^{2+} ions with an ionic radius of 0.69 Å were substituted with Zn^{2+} ions with a larger ionic radius of 0.74 Å and also because of the substitution of a less electronegative zinc metal (Zn:1.65, Ni:1.91) in the crystal lattice (Fig. 3a). The FWHM of (100) diffraction line tends to increase with an increase in the percentage of zinc additive and the d_{100} (Ni-Ni distance within the layers) decreases with an increase in the percentage of zinc additive; however, they do not vary with pH (Fig. 3b).

FTIR analysis: The infrared spectrum was obtained using a Thermo Nicolet, Avatar 370 using DTGS detector in the region 4000-400 cm^{-1}. A sharp peak observed in the region 3300-3700 cm^{-1} for all samples confirms the presence of the product β-$Ni(OH)_2$ [23], while for the α-phases, the disappearance of the narrow line at 3641 cm^{-1} indicates the formation of H-bonds. However, the α-phase was represented by the presence of a very broad absorption peak around 3500 cm^{-1} [24]. The appearance of large bands around 3417 and 1632 cm^{-1} were due to the $\nu(H_2O)$ stretching vibration and the $\delta(H_2O)$ bending vibration of water molecules indicating the presence of a certain amount of water molecules adsorbed on the nickel hydroxide materials (Table-3). The intensity of these two bands

TABLE-2
FWHM, d-VALUES AND PEAK INTENSITY IN (001), (100) AND (101) DIFFRACTION LINES OF β-$Ni(OH)_2$ SAMPLES

Sample	(001), c_0			(100), α			(101)		
	FWHM (°)	d (nm)	Peak intensity (count s^{-1})	FWHM (°)	d (nm)	Peak intensity (count s^{-1})	FWHM (°)	d (nm)	Peak intensity (count s^{-1})
A	0.631	2.328	275	0.244	7.156	601	1.440	1.065	740
B_1	1.866	0.787	160	0.249	7.012	396	0.615	2.495	385
B_2	1.500	0.979	181	0.249	7.012	400	0.592	2.592	381
B_3	1.409	1.042	152	0.249	7.012	376	0.579	2.650	386
B_4	0.489	3.004	468	0.249	7.012	697	0.409	3.751	890
C_1	2.072	0.708	098	0.375	4.655	247	0.681	2.253	283
C_2	1.570	0.935	139	0.375	4.655	367	0.659	2.328	369
C_3	1.318	1.114	148	0.375	4.655	395	0.579	2.650	420
C_4	0.439	3.346	308	0.375	4.655	496	0.329	4.664	818
D_1	2.292	0.640	144	0.409	4.269	370	0.739	2.076	350
D_2	1.962	0.748	115	0.409	4.269	317	0.679	2.259	310
D_3	0.989	1.485	210	0.409	4.269	460	0.579	2.650	558
D_4	0.409	3.591	604	0.409	4.269	762	0.306	5.014	1361
E_1	2.464	0.596	109	0.659	2.649	242	1.069	1.435	232
E_2	2.213	0.663	091	0.659	2.649	190	0.963	1.593	216
E_3	1.318	1.114	167	0.659	2.649	402	0.654	2.346	460
E_4	0.409	3.591	425	0.659	2.649	660	0.386	4.048	1100

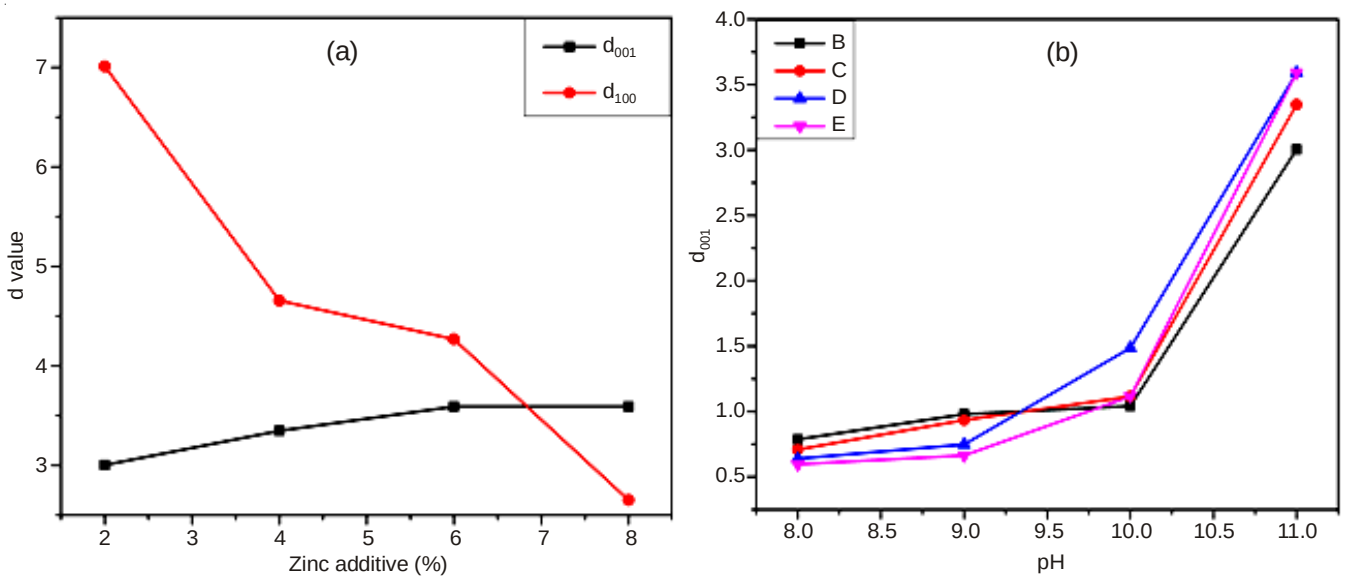

Fig. 3. Effect of (a) zinc content, B: 2 wt %; C: 4 wt %; D: 6 wt %; E: 8 wt % (b) pH on d_{001} value

TABLE-3
ASSIGNMENTS OF THE ABSORPTION BANDS FROM THE INFRARED SPECTRA

Wave numbers (cm^{-1})	Assignments of the absorption bands
3641	Vibrational stretching of hydroxyl group in the $Ni(OH)_2$ lattice ν(OH)
3417	Vibrational stretching of hydroxyl group of the adsorbed water ν(H_2O)
1632	Bending vibration of water molecules δ(H_2O)
1382 and 1047	Carbonate anion (1382-anti- symmetric stretching and 1047-symmetric stretching)
1141, 933 and 600	Sulphate anion (1141-anti-symmetric stretching, 933- Symmetric stretching and 600-anti-symmetric bending)
515	Lattice vibration δ(OH)
460	Ni-O lattice vibration ν(Ni-O)

of water molecules decreases with increasing pH values, suggesting that the content of the adsorbed water in $Ni(OH)_2$ samples decreases with an increase in pH value. This result was further corroborated by thermogravimetry and differential thermogravimetric studies. The presence of carbonate and sulphate ions was observed in the range of 1400-500 cm^{-1}. The bands at 1141, 933, 600 cm^{-1} and at 1382 and 1047 cm^{-1} are characteristics of SO_4^{2-} and CO_3^{2-} ions respectively as seen in Table-3.

The metal salt solution ($NiSO_4$) used for the precipitation was the origin of SO_4^{2-} anions, whereas the evolution of CO_3^{2-} anions was led by the dissolution of CO_2 in the air during synthesis. These anions are mainly adsorbed on the nickel hydroxide grain surface because the value of c_0 parameter of β-$Ni(OH)_2$ does not allow the presence of the anions intercalated between $Ni(OH)_2$ slabs. However, for SO_4^{2-} ion intercalation, a much closer interslab distance (9 Å) is preferred [25]. Samples prepared at a low pH exhibited the largest intensity as evidenced through IR spectrum for SO_4^{2-} ion, while there was hardly any appearance of CO_3^{2-} ion bands. On the other hand, samples prepared at higher pH values showed a decrease in the intensity of SO_4^{2-} bands but the CO_3^{2-} bands were highly apparent and increased with increasing pH values. Further, the spontaneous exchange of SO_4^{2-} for CO_3^{2-} ions can occur in agreement with an increase in pH values and with the adsorption selectivity of the anions, as CO_3^{2-} is preferred to other anions in $Ni(OH)_2$ [26]. Sample A did not show any sign of variation in the sulphate ion content for $Ni(OH)_2$ powders at a higher pH value. Likewise, as the pH values increased, the intensity of lattice vibration band δ(OH) also increased indicating that in the synthesized $Ni(OH)_2$ samples, the enhancement of Ni composition was certain which was further corroborated by TG and DTG studies.

Thermogravimetic analysis: TG and DTG studies of all samples were carried out using Perkin Elmer, Diamond model in the region from 0 to 750 °C which had a sensitivity of 0.2 mg. TG and DTG analyses were carried out to investigate the weight loss, dehydration and decomposition reaction of nickel hydroxide. Figs. 4 and 5 shows the TG and DTG curves of $Ni(OH)_2$ samples A and B_1-B_4.

However, the TG and DTG curves of all the samples revealed two obvious weight loss regions: a first region below 200 °C (between room temperature and 200 °C); and a second region between 200 and 450 °C. These two regions were distinctly shown in the DTG curve as two peaks: a broad peak and a sharp peak corresponding to the first and second regions respectively. Based on the observed weight loss steps in the experiments, two chemical reactions were postulated *i.e.* dehydration corresponding to the first weight loss of nickel hydroxide below 200 °C (eqn. 3); and decomposition of nickel hydroxide to nickel oxide (eqn. 4), corresponding to the second weight loss from 200 to 400 °C.

Dehydration reaction:

$$Ni(OH)_2 \cdot XH_2O \longrightarrow Ni(OH)_2 + XH_2O \quad (3)$$

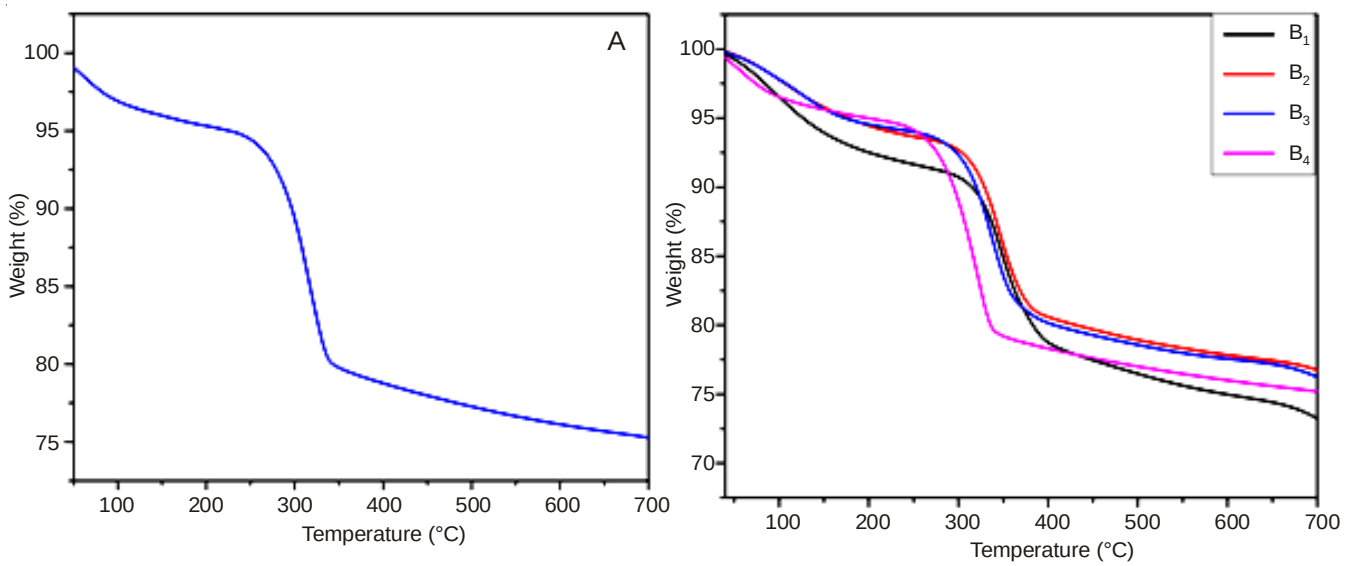

Fig. 4. Thermogravimetric analysis plots of $Ni(OH)_2$ samples A and (B_1-B_4)

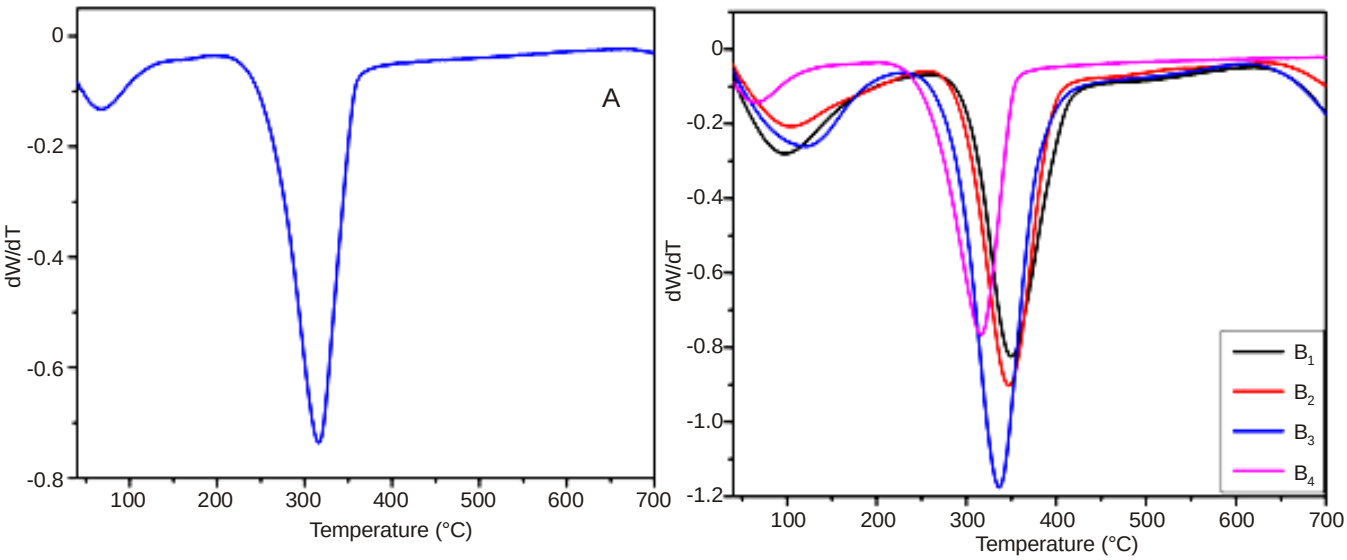

Fig. 5. Differential thermogravimetric analysis plots of $Ni(OH)_2$ samples A and (B_1-B_4)

Decomposition reaction:

$$Ni(OH)_2 \longrightarrow NiO + H_2O \quad (4)$$

The TG and DTG curves of samples prepared at low pH showed a broad peak compared to the samples prepared at higher pH because of higher water content. Further, as pH values increased, the water content decreased. For samples prepared at higher pH values, a decrease in the height of first weight loss step in DTG curves were observed. In addition, an increase in the pH decreases the weight loss percentage in dehydration step (Table-4). The adsorption of water was further confirmed by IR spectra.

It has been noted by several investigators that water in nickel hydroxide can either be adsorbed or structurally bonded between the $Ni(OH)_2$ lattices [7,27]. The interplanar distances are altered by this structurally bonded water (*i.e.* intercalated water) in the crystal structure, resulting in an expansion of "c-axis" from 4.6 Å for β-$Ni(OH)_2$ to approximately 8 Å for fully hydrated α-$Ni(OH)_2$ [28]. The present study indicates that there is no expansion of "c-axis" in the hydrated β-phase, thus indicating that the $Ni(OH)_2$ lattice has only adsorbed water without any structural bonding in β-$Ni(OH)_2$. All nickel hydroxide samples synthesized in this study had a β-phase structure and were substantiated by X-ray diffraction and infrared studies. These materials can only adsorb water molecules excluding the intercalation with a minimum distance of 4.6 Å. From TG and DTG curves, it can be clearly noted that the percentage weight loss is more in those samples prepared at higher pH and the $Ni(OH)_2$ concentration (*i.e.*, Ni composition) in active materials also increased with pH. A relationship between the decomposition temperature and the crystallite size of nickel hydroxide materials was established by Watanabe *et al.* [29]. Based on this fact, the low thermal stability of β-$Ni(OH)_2$ sample will be helpful in the electrochemical activity in determining the samples prepared at higher pH. The relationship between tapping density and decomposition temperature

TABLE-4
PERCENTAGE LOSS IN DEHYDRATION AND DECOMPOSITION REACTION, DECOMPOSITION TEMPERATURE AND TAPPING DENSITY OF SAMPLES A, B_1-B_4, C_1-C_4, D_1-D_4 AND E_1-E_4

Name of the sample	Percentage of loss		Decomposition temperature (°C)	Tapping density (g/cm^3)
	Dehydration (20-200 °C)	Decomposition (200-400 °C)		
A	4.38 %	19.2 %	315.35	1.009

Name of the sample		B_1	B_2	B_3	B_4	C_1	C_2	C_3	C_4
Percentage loss	Dehydration (20-200 °C)	6.89	5.53	5.35	4.71	7.27	7.21	6.20	4.53
	Decomposition (200-400 °C)	16.58	16.85	17.00	17.19	14.60	15.89	16.33	17.48
Decomposition temperature (°C)		349.36	346.34	332.41	312.16	347.70	333.14	332.74	312.75
Tapping density (g/cm^3)		1.455	1.442	1.373	0.986	1.642	1.362	1.144	1.044
Name of the sample		D_1	D_2	D_3	D_4	E_1	E_2	E_3	E_4
Percentage loss	Dehydration (20-200 °C)	7.96	7.69	6.47	3.43	9.49	7.51	5.77	4.94
	Decomposition (200-400 °C)	16.66	16.75	17.30	17.39	17.20	17.67	17.77	18.50
Decomposition temperature (°C)		346.23	337.18	332.12	321.19	356.86	335.95	332.37	314.19
Tapping density (g/cm^3)		2.262	1.458	1.090	0.880	1.774	1.605	1.156	0.982

indicates that with decreasing tapping density, synthesized nickel hydroxide materials became thermally less stable, as reflected in the higher decomposition reaction rate and lower decomposition temperature. It shows that the pH values increase during the preparation of β-$Ni(OH)_2$, while the decomposition and tapping density of β-$Ni(OH)_2$ decreases.

Cyclic voltammetry and EIS measurements: The representative CV curves for samples A-E are illustrated in Fig. 6 with varied scan rates. It is evident that an increase in the scan rate from 0.05 to 0.5 V/s, increases the oxidation and reduction peaks for samples B, C, D and E. However, the oxidation and reduction peaks disappear for sample A, with rising scan rates, along with an increase in the reversibility with addition of zinc. In general, as an estimate of the reversible potential for nickel electrodes, the average of the cathodic and anodic peak potentials (E_{rev}) are taken. However, the potential difference ($\Delta E_{a,c}$) between the anodic (E_a) and cathodic (E_c) peak potentials were determined by the reversibility of the redox reaction [30,31].

The comparative cyclovoltammetric results of electrodes A-E at a scan rate of 0.05 V/s are tabulated in Table-5. The experimental data shows that the redox reactions are somewhat quasi-reversible for all electrodes as indicated by the moderately large $\Delta E_{a,c}$. However, the $\Delta E_{a,c}$ of electrode C is only 369 mV, which is smaller than that of other electrodes as seen in Table-5. This indicates that the charge and discharge process of the electrode C is better reversible than other electrodes. It is well recognized that the electrochemical reaction process of a nickel hydroxide electrode is limited by proton diffusion through the lattice [32,33]. Therefore, it is of great importance to study the nickel electrode's proton diffusion coefficient.

TABLE-5
POTENTIAL VALUES OF CYCLIC VOLTAMMETRY CHARACTERISTIC FOR SAMPLES A-E

Sample	E_a (mV)	E_c (mV)	$E_{a,c}$ (mV)	$D \times 10^{-10}$ (cm^2/s)
A	126	-531	657	1.788
B	177	-196	375	2.280
C	174	-185	369	2.752
D	309	-101	410	2.596
E	360	-111	471	2.434

According to the Randlese Sevcik equation [32], the peak current is represented by

$$i_p = 2.69 \times 10^5 \times n^{3/2} \times A \times D^{1/2} \times C_0 \times \nu^{1/2} \quad (5)$$

where electron number of the reaction, surface area of the electrode, diffusion coefficient, scanning rate and initial concentration of the reactant are denoted by n, A, D, ν and C_0 respectively.

For the β-$Ni(OH)_2$ electrode:

$$C_0 = \rho/M \quad (6)$$

where the theoretical density of β-$Ni(OH)_2$ and the molar mass of $Ni(OH)_2$ are represented by ρ and M respectively. From eqn. 5, for sample C and D, the proton diffusion coefficients are calculated to be 2.752×10^{-10} cm^2 s^{-1} and 2.596×10^{-10} cm^2 s^{-1} which are larger as compared to samples A, B and E.

Electrochemical impedance spectroscopy (EIS) is an effective parameter for analyzing the internal structures and structural change during cycling [34]. Fig. 7 represents the electrochemical impedance spectra of the $Ni(OH)_2$ electrodes A-E. The impedance spectra of all these electrodes display a depressed semicircle considerable from charge transfer resistance in the high-frequency region corresponding to charge transfer resistance (R) in parallel connection with the capacitance (C) and the line at low frequency regions corresponds to Warburg impedance (Z) of proton diffusion [35,36]. A proposed equivalent circuit for the frequency response of the $Ni(OH)_2$ electrodes A-E is given in Fig. 8. A decrease in the charge transfer resistance and an increase in the capacitance with zinc additive indicates that there is an improvement in the surface electrochemical activity of $Ni(OH)_2$ electrode.

Conclusion

In the present study, $Ni(OH)_2$ materials were synthesized by co-precipitation method with zinc additive. The obtained samples were in β-form with a Brucite-type structure and a hexagonal unit cell. With increasing zinc additive in the β-$Ni(OH)_2$ samples, the d_{001} and d_{101} diffraction lines increased because of the substitution of Ni^{2+} by Zn^{2+} of a larger ionic radius and lower electronegativity. Similarly, the d_{001} and d_{101} also increased with pH, while d_{100} diffraction line decreased

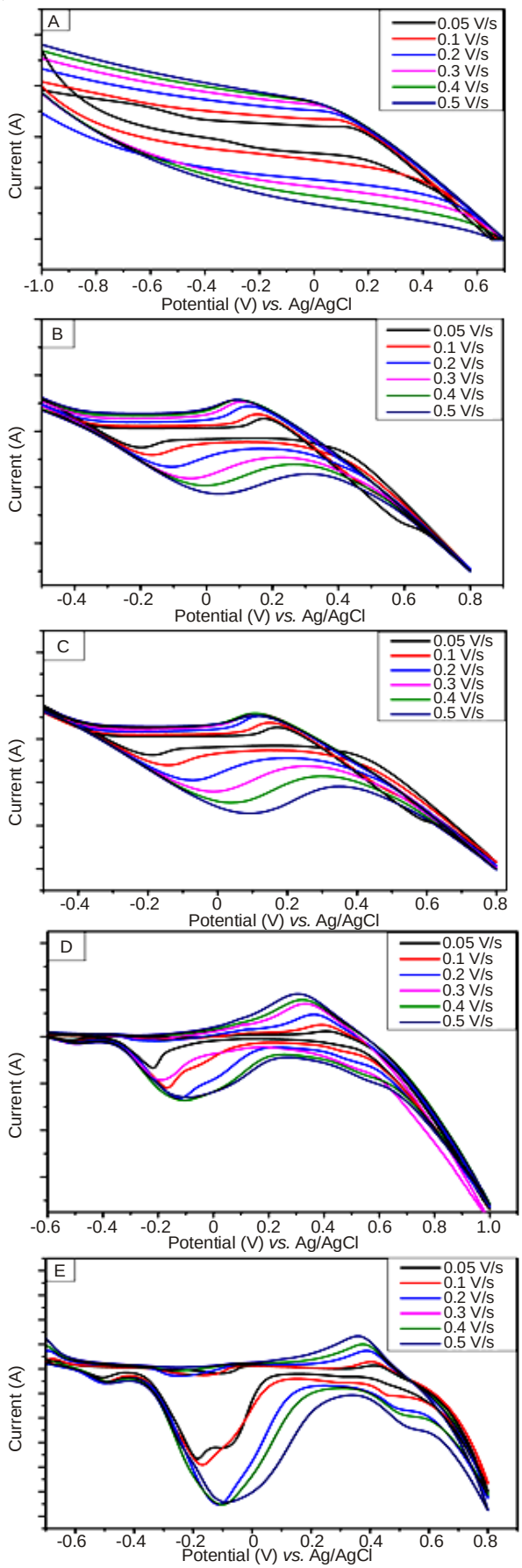

Fig. 6. Cyclic voltammograms of $Ni(OH)_2$ electrodes, A: 0 wt % Zn; B: 2 wt % Zn; C: 4 wt % Zn; D: 6 wt % Zn; E: 8 wt % Zn; at various scan rates

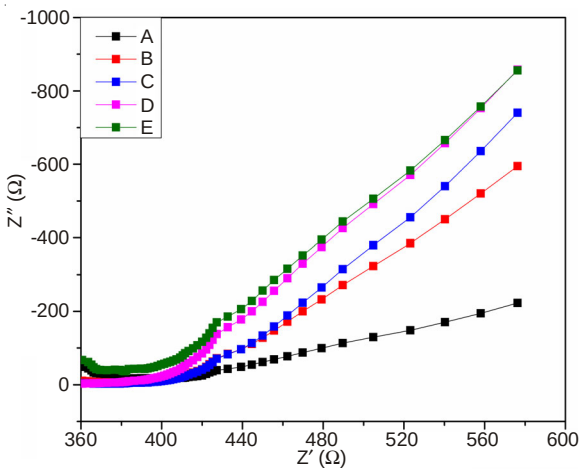

Fig. 7. Electrochemical impedance spectra of $Ni(OH)_2$ electrodes A-E

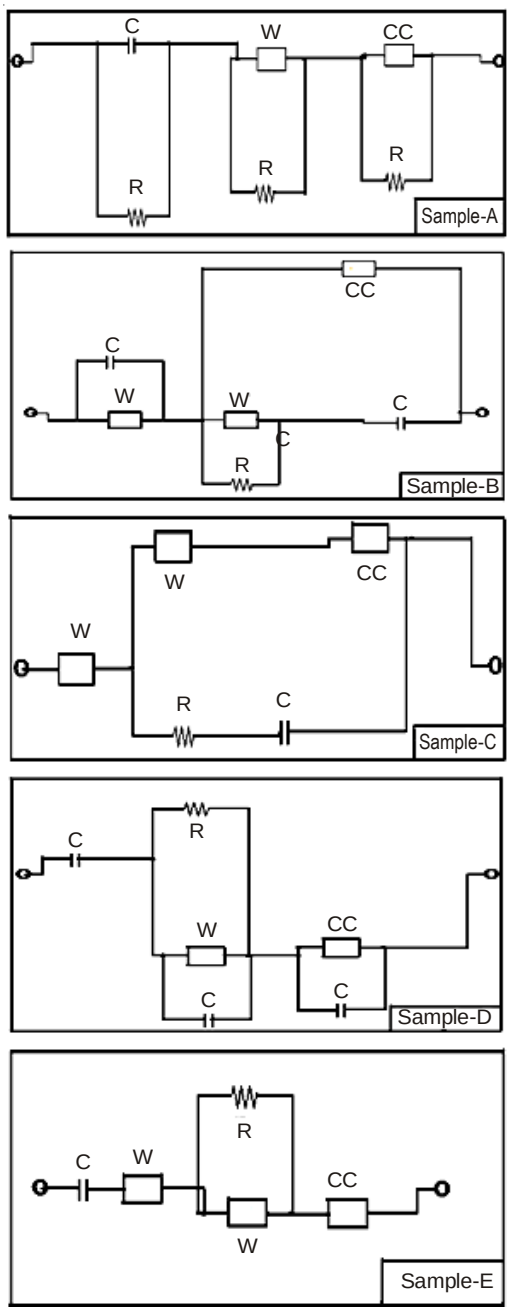

Fig. 8. Proposed equivalent circuits of $Ni(OH)_2$ electrodes A-E

with zinc additive. The degree of ordering and crystallinity of β-$Ni(OH)_2$ sample increased with increase in pH. The SO_4^{2-}, CO_3^{2-} and H_2O molecules were adsorbed in the crystals and the adsorption of SO_4^{2-} and H_2O molecules decreased with increasing pH. However, the amount of CO_3^{2-} adsorption increased with increasing pH. Finally, the thermal stability and tapping density decreased with increasing pH and the nickel composition was found to be higher in samples prepared at higher pH values. Cyclic voltammetry studies revealed that higher performance was observed in electrodes with zinc-ion additive. However, these electrodes exhibited improved reversibility through a reduction in the difference between oxidation and reduction potentials. Decreasing the charge transfer resistance and increasing the capacitance with zinc additive leads to higher surface electrochemical activity of $Ni(OH)_2$ electrode.

ACKNOWLEDGEMENTS

One of the authors (RCR) thank Sophisticated Test and Instrumentation Centre, Cochin, India for TG-DTG analysis, Indian Institute of Science, Bangalore, India for providing EDAX analysis, BIT, Bangalore, India for FT-IR analysis and Central College, Bangalore, India for XRD analysis.

REFERENCES

1. C. Delmas, C. Faure, L. Gautier, L. Guerlou-Demourgues and A. Rougier, *Philos. Trans. R. Soc. London Ser. A*, **354**, 1545 (1996).
2. G. Halpert, in eds.: D.A. Corrigan and A.H. Zimmerman, Nickel Hydroxide Electrodes, PV 90-4, The Electrochemical Society Proceedings Series, Pennington, NJ, p. 1 (1990).
3. J. McBreen, in eds.: R.E. White, J.O.M. Bockris and B.E. Conway, Modern Aspects of Electrochemistry, Plenum Press, New York, Vol. 21, p. 29 (1990).
4. H. Bode, K. Dehmelt and J. Witte, *Electrochim. Acta*, **11**, 1079 (1966).
5. D.A. Corrigan and S.L. Knight, *J. Electrochem. Soc.*, **136**, 613 (1989).
6. R. Barnard, C.F. Randell and F.F. Tye, *J. Appl. Electrochem.*, **10**, 109 (1980).
7. C. Faure, C. Delmas and M. Fouassier, *J. Power Sources*, **35**, 279 (1991).
8. L. Guerlou-Demourgues, *J. Electrochem. Soc.*, **143**, 561 (1996).
9. P. Oliva, J. Leonardi, J.F. Laurent, C. Delmas, J.J. Braconnier, M. Figlarz, F. Fievet and A. Guibert, *J. Power Sources*, **8**, 229 (1982).
10. M. Oshitani, M. Watada, T. Tanaka and T. Iida, in eds.: P.D. Bennett and T. Sakai, Hydrogen and Metal Hydride Batteries. PV 94-27, The Electrochemical Society Proceedings Series, Pennington, NJ, p. 303 (1994).
11. S. Begum, V. Muralidharan and C. Ahmedbasha, *Int. J. Hydrogen Energy*, **34**, 1548 (2009).
12. H.K. Liu, B. Bright, C.Y. Wang, M. Lindsay and S. Zhong, *J. New Mater. Electrochem. Systems*, **5**, 47 (2002).
13. J. Chen, D.H. Bradhurst, S.X. Dou and H.K. Liu, *J. Electrochem. Soc.*, **146**, 3606 (1999).
14. Z. Chang, G. Li, Y. Zhao, Y. Ding and J. Chen, *J. Power Sources*, **74**, 252 (1998).
15. M.V. Vázquez, M.J. Avena and C.P. De Pauli, *Electrochim. Acta*, **40**, 907 (1995).
16. L. Indira, M. Dixit and P.V. Kamath, *J. Power Sources*, **52**, 93 (1994).
17. Q. Song, Z. Tang, H. Guo and S.L.I. Chan, *J. Power Sources*, **112**, 428 (2002).
18. K. Watanabe and N. Kumagai, *J. Power Sources*, **76**, 167 (1998).
19. T.N. Ramesh and P.V. Kamath, *Mater. Res. Bull.*, **43**, 2827 (2008).
20. C. Tessier, P.H. Haumesser, P. Bernard and C. Delmas, *J. Electrochem. Soc.*, **146**, 2059 (1999).
21. S. Deabate, F. Fourgeot and F. Henn, *J. Power Sources*, **87**, 125 (2000).
22. T.N. Ramesh, R.S. Jayashree and P.V. Kamath, *J. Electrochem. Soc.*, **150**, 520 (2003).
23. R. Acharya, T. Subbaiah, S. Anand and R.P. Das, *J. Power Sources*, **109**, 494 (2002).
24. M. Rajamathi, P.V. Kamath and R. Seshadri, *J. Mater. Chem.*, **10**, 504 (2000).
25. L. Guerlou-Demourgues, C. Denage and C. Delmas, *J. Power Sources*, **52**, 269 (1994).
26. E. Shangguan, Z. Chang, H. Tang, X.-Z. Yuan and H. Wang, *Int. J. Hydrogen Energy*, **35**, 9716 (2010).
27. B. Mani and J.P. Neufville, *J. Electrochem. Soc.*, **135**, 800 (1988).
28. M. Vidotti, R. Salvador and S. Cordobadetorresi, *Ultrason. Sonochem.*, **16**, 35 (2009).
29. K. Watanabe, T. Kikuoka and N. Kumagai, *J. Appl. Electrochem.*, **25**, 219 (1995).
30. W.G. Zhang, W.Q. Jiang, L.M. Yu, Z.Z. Fu, W. Xia and M.L. Yang, *Int. J. Hydrogen Energy*, **34**, 473 (2009).
31. L. Bing, Y. Huatang, Z. Yunshi, Z. Zuoxiang and S. Deying, *J. Power Sources*, **79**, 277 (1999).
32. A.H. Zimmerman and P.K. Effa, *J. Electrochem. Soc.*, **131**, 709 (1984).
33. X. Cao, J. Wei, Y. Luo, Z. Zhou and Y. Zhang, *Int. J. Hydrogen Energy*, **25**, 643 (2000).
34. V. Subramanian, V. Boovaragavan, K. Potukuchi, V. Diwakar and A. Guduru, *Electrochem. Solid-State Lett.*, **10**, 25 (2007).
35. V. Mancier, A. Métrot and P. Willmann, *Electrochim. Acta*, **41**, 1259 (1996).
36. B. Liu, H.T. Yuan and Y.S. Zhang, *Int. J. Hydrogen Energy*, **29**, 453 (2004).